Agricultural and Forest Meteorology 373 (2025) 110713

Contents lists available at ScienceDirect

Agricultural and Forest Meteorology

journal homepage: www.elsevier.com/locate/agrformet

Using high penetration airborne LiDAR and dense UAV scanning to produce accurate 3D maps of light availability in dense tropical forest

Vincyane Badouard [a,b], Philippe Verley [a], Yuchen Bai [a,c], Giacomo Sellan [b], Léa Françoise [d], Eric Marcon [e], Géraldine Derroire [b,f,g], Grégoire Vincent [a,*]

[a] AMAP, ADEME, CIRAD, CNRS, INRAE, IRD, Université de Montpellier, Montpellier, France
[b] Cirad, UMR EcoFoG (AgroParistech, CNRS, INRAE, French Guiana, Université des Antilles, Université de la Guyane), Campus Agronomique, Kourou, France
[c] CNRS, NRS, Inria, Grenoble INP, LJK, Université Grenoble Alpes, Grenoble, France
[d] CNRS, UMR EcoFoG (AgroParistech, CNRS, INRAE, French Guiana, Université des Antilles, Université de la Guyane), Campus Agronomique, Kourou, France
[e] AMAP, AgroParisTech, CIRAD, CNRS, INRAE, IRD, Université de Montpellier, Montpellier, France
[f] Cirad, UPR Forêts et Sociétés, University of Montpellier, Montpellier, France
[g] Department of Forestry, University of Brasilia, Campus Darcy Ribeiro, Brasília 70900-910, Brazil

ARTICLE INFO

Keywords:
Understory light
Light transmittance anisotropy
Raytracing model
ALS
UAV
Vertical light extinction profile
AMAPVox

ABSTRACT

LiDAR makes it possible to describe the 3D structure of the forest, from which species habitats can be accurately estimated, over large areas at fine resolution. However, standard airborne laser scanning (ALS) fails to describe the lower canopy in sufficient detail due to occlusion by the upper canopy. The understory is important to characterise as it harbours the majority of the forest community and is the place where regeneration takes place. Here we explored the potential of low altitude high power ALS with enhanced penetration, and denser UAV LiDAR (Unmanned Aerial Vehicle) to describe the structure of the understory. We used the recorded laser pulse extinction to build a 3D model of light transmission through the canopy. We evaluated the capacity of the light transmission model to estimate the spatial and angular variation of light in the tropical understory, considering different leaf inclination distribution functions (LIDF), compared with measurements from two different field sensors. We found that (i) LiDAR can be used to estimate the light environment in the understory in a spatially and angularly consistent way; (ii) high pulse density does not guarantee an accurate characterization of the forest structure, and penetration rate is an important characteristic to accurately describe the forest structure, especially the understory; (iii) taking into account the anisotropic nature of light transmittance improved the estimation of absolute light levels by radiative transfer.

1. Introduction

Light is required for the development of all photosynthetic plants, and light level influences plant growth (Nicotra et al., 1999; Scanga, 2014; Shirley, 1929) and survival (Nicotra et al., 1999; Osunkoya, 1992). In a forest, the opening of a gap creates a sudden increase in the light level reaching the ground and triggers a new cycle of plant succession (Clements, 1916; Finegan, 1996). This drives the recruitment of plant species and recolonisation by fauna (Denslow and Gomez Diaz, 1990; Fortunel et al., 2016; Shirley, 1929). The strong vertical gradient in light availability in closed canopy forest fosters species coexistence through differentiation of niches (Laurans et al., 2014), contributing to maintaining high species diversity (Terborgh, 1985). The availability of light therefore drives the spatial distribution of plant species according to their tolerance to shade (Poorter and Arets, 2003) and also through the influence of light on plant-fungi interactions (Nagata et al., 2015) and on litter decomposition (Wang et al., 2021). Light also influences the distribution of animal species according to their light needs for vision, communication, hunting, reproduction, defence and camouflage, and so the effectiveness of plant-animal interactions (Théry, 2001); review in (Endler, 1993). Light also strongly influences forests' temperature and humidity (Baraloto and Couteron, 2010; Thom et al., 2020; Tymen et al., 2017). As a result, light also influences the distribution of organisms sensitive to those atmospheric characteristics, such as amphibians and

* Corresponding author.
E-mail addresses: vincyane.badouard@gmail.com (V. Badouard), philippe.verley@ird.fr (P. Verley), yuchen.bai@inria.fr (Y. Bai), giacomo.sellan@cirad.fr (G. Sellan), lea.francoise@cnrs.fr (L. Françoise), eric.marcon@agroparistech.fr (E. Marcon), geraldine.derroire@cirad.fr (G. Derroire), gregoire.vincent@ird.fr (G. Vincent).

https://doi.org/10.1016/j.agrformet.2025.110713
Received 30 October 2024; Received in revised form 19 June 2025; Accepted 24 June 2025
Available online 15 July 2025

reptiles (Berezowski et al., 2015; Halverson et al., 2003). For foresters, characterising light can guide management practices, such as thinning or planting, aimed at optimising tree growth conditions according to the management objectives (conservation, production, etc.) (Aussenac, 2000).

Different methods have been used to characterise the light environment in the forest. Light availability below the canopy can be estimated by (i) a visual description of the tree's exposition such as the Dawkins' crown illumination index (Collinet, 1997), (ii) using sensors like PAR sensors, solarimeters or lux metres (Laurans, 2013; Nicotra et al., 1999), hemispherical photographs (Chazdon and Field, 1987) or other detectors (Engelbrecht and Herz, 2001; Ferment et al., 2001; Yoda, 1974). Such measurements need to be repeated across the study area to characterise its spatial heterogeneity. The development of automatic sensors able to independently collect and store measurements in the field has greatly improved the characterisation of the micro-environment by allowing its continuous and long term monitoring (Bramer et al., 2018; Engelbrecht and Herz, 2001). The disadvantage of fixed sensors remains the number of sensors needed to cover the study area when studying the spatial variability of light (see SI Table S1 for the review of different light measurement methods).

The emergence of LiDAR technology in the late 1990s made it possible to capture important features of the 3D forest structure, which have been used to develop statistical models of the microclimate over extensive areas at fine resolution (Bramer et al., 2018; Jucker et al., 2018; Lenoir et al., 2017; Zellweger et al., 2019b).

From the LiDAR data describing the 3D structure of the forest, one can derive various features to characterise the variation in the light environment at different spatial and temporal scales. The Canopy Height Model (CHM) provides information about the forest canopy height which can be assumed to be inversely related to available light at ground level (Zellweger et al., 2019b). Other elements of the forest structure are used as proxies of the available light, such as the size and distribution of gaps and the distance to the gap (Gaquière, 2024; Goulamoussène et al., 2017), or canopy structural complexity indices (Atkins et al., 2018). Synthetic hemispherical images (Moeser et al., 2014; Zellweger et al., 2019a) derived from LiDAR allow to compute the global and diffuse site factor (Becker et al., 1989) to characterise local light availability (see SI Table S2 for a review of the LiDAR products used to estimate light environment). However, while synthetic hemispherical photos may be simulated at any height in the canopy (as opposed to real hemispherical photos taken close to the ground), they remain point measurements and do not provide a 3D spatially continuous representation of light availability.

Various models relying on LiDAR-derived data have been developed to study light extinction through the forest canopy (Hovi et al., 2024; Nyman et al., 2017; Peng et al., 2014; Van der Zande et al., 2011; Vincent et al., 2023; Witzmann et al., 2024; Xue et al., 2022). Most of those models integrate the sun's changing position over daily and yearly time, the vertical forest structure and the direct and diffuse light to compute light environment. They are briefly reviewed here.

Van der Zande et al. (2011) use simulated terrestrial LiDAR measurements of virtual monospecific forest stands of three tree species ((a) *Fagus sylvatica*, (b) *Platanus* × *acerifolia*, and (c) *Populus nigra*). They simulate light absorption using a physically based ray tracing model, setting average leaf level transmittance and reflectance values, both on detailed mock-ups and the simplified voxelized scenes derived from the LiDAR data. The main difference between the two scenes lies in the representation of leaves: in the voxelized scene, leaves are modelled as discs, each with a fixed area of 0.01 m^2, a random azimuth angle, and a zenith angle that corresponds to the average zenith angle for the tree species simulated. They report a high level of consistency between detailed and simplified mock-ups with an overestimation of the mean transmittance profile ranging from 3 to 12 % depending on the species and the simulated LAI level (which varied from 2 to 6). Peng et al. (2014) use the LiDAR-derived canopy height model to calculate the path length of sun rays through a real forest dominated by *Picea crassifolia*. The input data of the model are the CHM, the under-branch height layer measured from the ground (the combination of which provides the local canopy depth), the Digital Elevation Model (DEM), and solar position file (azimuth and altitude angles). They adjust the mean canopy extinction coefficient to match pyranometer readings taken above and below the canopy approximating the leafy canopy to a turbid medium (Beer Lambert approximation). Nyman et al. (2017) test different radiation models in Eucalyptus forests, two of which use LiDAR and explicitly include path length of the transmitted light (i) The path length model (PL model) defines transmission as a function of the path length of a directional beam through the canopy. Trees height is acquired by LiDAR and the extinction coefficient is calibrated with field measurements of radiation, much like in the Peng et al. (2014) model. (ii) The Light Penetration Index (LPI) model is based on the LPI, obtained directly from airborne LiDAR point clouds as the ratio of ground returns to the total number of returns. LPI is used as an estimate of canopy transmittance. The LPI model was found to be biased in dense forest whereas the PL model demonstrated better accuracy, but the latter required the calibration of an extinction coefficient. Witzmann et al. (2024) also use the Beer-Lambert approach to compute light reaching the forest floor. The path length through the canopy is derived from beam direction and the canopy height model. They use a light extinction coefficient derived from the literature based on the dominant plot species composition. Xue et al. (2022) derive from an airborne LiDAR scan of regularly aligned trees in small stands, a meshed geometric representation of the 3D canopy structure and use it to simulate transmission and reflection of shortwave radiation inside the forest canopy. Individual tree crowns are modelled as semi-ellipsoids for broadleaves and cones for conifers. The optical properties, including reflectance and transmittance, derived from the literature are applied to the triangulated crown surfaces to simulate radiation within the forest canopy. More complex light transmission models such as the 3D Discrete Anisotropic Radiative Transfer (DART) (Gastellu-Etchegorry et al., 2016) model or PARAS (Hovi et al., 2024) were tested to compute canopy transmittance per spectral range. The modelling strategy presented in Hovi et al. (2024) requires abundant data collection and is not easily applicable beyond plot scale. Terrestrial laser scanning (TLS) is used to describe individual tree crowns in 3D, hemispherical photographs are used to estimate plot level PAI (i.e. plant area index), and reflectance of the foliage of the different species and of woody elements and the forest floor, have to be made using a field spectrometer. All these models (except the DART parameterisation used in (Hovi et al., 2024)), assume isotropy (i.e. property of being independent on direction) of light transmittance within the canopy. Yet various studies have shown that the angular distribution of leaves is an important parameter for light transmission and reflection through the forest canopy (Myneni and Ross, 1989; Pisek et al., 2013) and that the plagiophile distribution (i.e. leaves are predominantly oriented at oblique angles to the horizontal plane) is probably more relevant than the spherical distribution (i.e. leaves have no preferred orientation) for most deciduous species (Pisek et al., 2013). The angular distribution of leaves is indeed not random, as plants orientate their leaves to reduce self-shading and maximise light interception and hence reduce light competition (Yang et al., 2023).

In the present study we use the AMAPVox software which was first introduced in (Vincent et al. 2017) to compute PAI from Airborne Laser Scanning (ALS) data. AMAPVox calculates the light attenuation by tracing each transmitted pulse through a 3D grid and allows for the specification of different Leaf Inclination Distribution Functions (LIDF). Leaf inclination is then used to compute light transmittance from various angles of incident light. AMAPVox is highly scalable and can be used to process TLS or ALS data, and applicable to single or multiple return systems. No calibration data is required, nor does the species specific information about foliage density or optical properties - which remains unavailable for highly diverse tropical forests. It does not require prior segmentation of the forest canopy into individual tree crowns which is

still a very challenging task in tall dense forests (Aubry-Kientz et al., 2019). However, it does rely on sufficiently dense LiDAR sampling throughout the entire canopy to characterise the LiDAR signal extinction pattern down to the forest floor.

A general characteristic of aerial LiDAR is the gradual extinction of the signal along the different forest layers traversed. This leads to a low sampling intensity of the lower canopy (Brede et al., 2022). To circumvent this limitation, terrestrial LiDAR (TLS) can be used, but TLS cannot easily cover large areas. Scanning one ha of dense tropical forest typically requires a week or two of intensive fieldwork as the scanner has to be moved from one scan location to the next (Tao et al., 2021). The Mobile Laser Scanner (MLS) which can be carried along by a person walking in the forest, is much faster to operate and has the additional advantage to reduce occlusion by multiplying viewpoints (Bauwens et al., 2016). However, to our knowledge the MLS systems currently on the market do not provide all the scanning geometrical characteristics needed to reconstruct the optical paths of all the emitted pulses. Lightweight LiDAR scanners on board Unmanned Aerial Vehicles (UAV) are also commonly used to scan areas up to a few tens of ha. They are more affordable than using a plane or a helicopter, and better suited to high frequency acquisitions (Anderson and Gaston, 2013).

Various aerial LiDAR acquisition parameters need to be considered to improve the effective sampling of the understory when scanning from above the canopy. A lower flight height reduces the footprint size and increases the detection rate by increasing irradiance. Those characteristics improve the signal penetration rate (proportion of returns reaching the ground) (Lee and Wang, 2013; Vincent et al., 2023). Increasing the optical power will also increase the penetration but this comes at the expense of a lower pulse repetition rate (PPR) as they are inversely related.

In this study, we test if lower flights, more penetrating (LiDAR operated on a plane) or denser (LiDAR operated on a UAV) airborne LiDAR can more effectively describe the light levels of the understory in dense tropical forest compared to high altitude ALS. The produced 3D light availability maps are then used to analyse the largely unexplored vertical structure of light in a dense tropical forest canopy. We address the following questions: (I) How precise (i.e. capable of detecting small changes in incident light across space) and how accurate (i.e. capable of predicting unbiased light penetration per incident angle) are light maps derived from airborne LiDAR? (II) Does taking into account the anisotropy of light transmittance improve the estimation of light? (III) To what extent do acquisition parameters such as pulse density and LiDAR penetration affect prediction accuracy (precision and bias) and what are recommended best practices? (IV) How variable is light availability vertically? Can ground based sensors inform on light availability higher up in the canopy?

2. Materials and methods

We use field-based measurements of light conditions as a ground-truthing to compare different LiDAR acquisitions, a more penetrating ALS or denser UAV, acquired at the same time.

2.1. Study site

This study was conducted at the Paracou field station (Latitude: 5.25 ′N, Longitude: 52.93′W), near Sinnamary, French Guiana.

The site is a lowland tropical rain forest with mean annual precipitation of 3041 mm. The forest in the area is dense (4730 stems bigger than 1 cm of diameter at breast height per ha) and its botanical composition highly diversified. The mean canopy height (computed by taking the highest point per m^2) is about 31 m and the basal area 31 m^2/ha (Huertas et al., 2022).

The study area where the different LiDAR sensors are compared is a 4-ha subplot located within a 25-ha permanent sample plot (P16). Topography is gentle as can be seen on the Digital Terrain Model (DTM) derived from LiDAR of the study area (SI Fig. S3).

2.2. Data acquisition

2.2.1. ALS aircraft laser scanning

ALS LiDAR data were acquired by the private company ALTOA (http://www.altoa.fr/) on the 26th of October 2023 around noon. The LiDAR sensor used was a RIEGL VQ 780 II mounted on a BN-2 Islander. ALS sensor specifications are given in Table 1. Point cloud classification (vegetation, ground, noise) was also performed by ALTOA.

We compared two ALS acquisition scenarios. Either flying at high altitude (1000 m AGL (Above Ground Level)) and using a high Pulse Repetition Rate (PPR), or flying lower (500 m AGL) and selecting a lower PPR which allows the transmission of higher energy pulses. The combination of lower flight height and higher power increased the laser pulse penetration rate (Table 1).

2.2.2. UAV unmanned aerial vehicle laser scanning

UAV LiDAR data were acquired on the 19th of October 2023. The scanner used was a Hovermap ST-X (Emesent Pty Ltd, Queensland, Australia) mounted on the Matrice 300 DJI drone. The UAV LiDAR produced extremely dense point clouds, but had a lower penetration than ALS. Details of the characteristics of the Hovermap ST-X are described in Table 1.

The Hovermap ST-X does not use a GPS but relies on the Simultaneous Localization and Mapping (SLAM) technology to determine its position relative to the take-off point. The flight plan consisted of parallel flight lines 10 m apart at 85 m AGL. We restricted the analysis to data points with scanning angles within ± 45° of vertical for the comparative analysis between sensors. However, we also used a larger swath angle (±70°) to demonstrate transmittance anisotropy taking advantage of the 360° x 40°Field Of View of the UAV LiDAR (See SI section *Anisotropy test*).

The 4-hectares study area was scanned in two successive flights, each completed in 20 min. The two flight plans had a 20 m overlap (see SI Fig. S1 for UAV flight plan). Flight and sensor specifications are described in Table 1.

The UAV point cloud classification (ground, noise vegetation) was conducted using lastools (ver. 231025).

Table 1
Characteristics of LiDAR acquisitions. AGL: Above Ground Level.

	High altitude (standard)	*Low altitude*	*UAV*
Scanner	Riegl VQ 780 II		Hovermap ST-X
Sensor			Hesai XT32M2X
Flight altitude AGL (m)	1000	500	85
Pulse frequency	1MHz	150kHz	340kHz
Flight speed	170km/h (47m/s)		5m/s
Beam divergence (mrad)	0.25 (measured at the 1/e2 point)		1.7 × 1.9
Footprint diameter at ground level (cm) at vertical	25	12.5	15
Density (±30°) (points/m^2)	344	46	2606 (±45°)
Density (±30°) (pulses/m^2)	222	25	4391 (±45°)
Average number of echoes per shot	2.3	3.2	1.5
Max number of echoes	11	14	3 (1st, last and strongest; fixed maximum number of returns)
Range (m) (10 % reflectivity of target, standard clear visibility (23 km)	1435	3115	80
Penetration rate (% of ground points in last echoes)	10	19	4 (±30°)
Average height (m) of the last echo	31.2	26.1	35.2

2.2.3. Light sensors (validation data)

Two types of light measurements were made in order to validate the light level predicted from the LiDAR data. Instantaneous recordings of blue light transmittance (to avoid multiple reflections) were made along two transects with an LAI2200C sensor (see below). In addition, continuous recordings of the luminous flux (lux) were made using 20 MX2022 HOBO sensors along one of the transects.

2.2.3.1. HOBO. The 20 HOBO Pendant MX2202 sensors were placed every 10 m along a transect line covering a topographic gradient (in the north - south direction). They were positioned horizontally one metre aboveground and fixed on plastic tubes. Sensor readings were taken every 15 min and individual records were summed per day and averaged over one year (from 01/04/2023 00:00:00 to 31/03/2024 24:00:00). The MX2202′s light sensor has a spectral response that closely matches the photopic response of the human eye. The response of this light metre is only roughly proportional to the cosine of the angle at which the light is incident. Angles beyond ± 20° from vertical show a marked decrease in sensitivity compared to the expected cosine response (https://www.onsetcomp.com/products/data-loggers/mx2202).

The data from HOBO No. 7 were excluded because it stopped collecting data before the end of the monitoring period.

2.2.3.2. LAI2200. We measured blue light (320–490 nm) at a height of 1 m above the ground, using two coupled mobile field sensors (LAI2200C, (LI-COR, Inc. 4647 Superior Street Lincoln, NE 68504-0425) (www.licor.com/lai)): one sensor was moved around to take measurements at 1 m aboveground below the canopy while another sensor was set-up in a large clearing (3000 m^2) located 1.5 km away from the centre of our region of interest. This reference sensor was mounted on a tripod and recorded light every 15 s. The measurements below the canopy were taken along two transects of different resolution for a total of 46 measurement positions: (i) 20 along the transect of the HOBO sensors which were placed every 10 m along a 190 m long line (*HOBO transect*) and (ii) 26 every 2 m along a 50 m long line on a footpath, including one position common to both transects. The second transect showed higher variation in the degree of canopy opening (*LAY transect*) (see SI Figs. S2 and S3 for the experimental design of LAI2200 sensors). Between two and four replicated LAI2200 measurements were taken in diffuse sunlight conditions, close to sunset (5:15–6:20 pm), within a week of the LiDAR acquisitions (October 2023) (21, 22 and 25/10/2023). Sensors were inter-calibrated before use by taking thirty-three measurements over a wide canopy opening gradient, during 30 min just after sunset (no direct sunlight) on the same day. A total of 765 LAI2200 measurements were taken below the canopy.

We computed transmittance values from the LAI2200 readings by dividing the measurements taken below the forest canopy by the measurements taken in the open at five incident angles, called rings (148° field-of-view) (Table 2).

2.2.3.3. Georeferencing. Under dense tree canopy, differential GPS systems do not allow submeter precision (Næsset and Jonmeister, 2002) and autonomous surveyor grade GPS do not even reach metre precision (Purfürst, 2022). The HOBO transect was laid out according to existing stakes and spatialized using a tape metre and a magnetic compass relative to the footpaths. The LAY transect is located on a footpath, begins at the intersection of two footpaths, and the distance between the sensors was measured with a tape metre. We therefore geolocated the field sensors based on the existing footpaths (visible on the LiDAR derived terrain model) and subplot corners (which had been geolocated previously using a total station).

Table 2
Angles of the five rings of the LAI2200C sensor.

Ring	Nominal Angular Coverage	Plane angle (θ)	Solid angle (Ω)
1	0.0 - 12.3°	12.3°	0.14 sr
2	16.7 - 28.6°	11.9°	0.50 sr
3	32.4 - 43.4°	11°	0.74 sr
4	47.3 - 58.1°	10.8°	0.94 sr
5	62.3 - 74.1°	11.8°	1.20 sr

2.3. Analyses

2.3.1. UAV LiDAR data processing

2.3.1.1. UAV point clouds correction and completion. Both UAV LiDAR point clouds were first processed using *Aura* proprietary software implementing a SLAM algorithm (Milton, QLD, Australia) into a geometrically consistent point cloud and exported in las format. As the las files format produced by the AURA software does not comply with ASPRS las standards, we recomputed the *NumberOfReturns, ReturnNumber, ScanAngle and gpstime* from the available data in the point cloud and the trajectory file. This post-processing of the las file was conducted in R using the lidR package (Roussel et al., 2020; 2024).

2.3.1.2. UAV point clouds alignment. Since the UAV point clouds were not georeferenced, we aligned them on the high density ALS point cloud. To do so, we thinned the point cloud (by the *lasthin* method in LAStools software (http://rapidlasso.com/LAStools)) by taking the highest return in each 10 cm grid cell. We applied the same thinning procedure to the high density ALS point cloud). The two UAV point clouds were first roughly aligned by hand on the high density ALS point cloud. We then used the Iterative Closest Point (ICP) algorithm in CloudCompare (https://www.cloudcompare.org) to finely match UAV top of canopy points with the ALS top of canopy. We later controlled the quality of the alignment by comparing the Digital Terrain Model at 1 m resolution derived from point clouds acquired by the two LiDAR sensors (the difference between the two DTMs in the 4 ha area is on average 0.03 m and the RMSE is 0.09 m). We applied the same transformation to the trajectories. UAV points clouds were then filtered by range excluding points closer than 2 m to remove points belonging to the drone and excluding scanning angles > 45° from vertical.

2.3.2. Light calculations

To map light availability in the forest we used the open source AMAPVox software v 2.3.1 ((Vincent et al., 2017); www.amapvox.org) following a two steps procedure. First the LiDAR pulse trajectories are analysed to estimate the light attenuation in each 1 m^3 cell of the 3D grid (voxel) (See SI Fig. S4 for an illustration of the voxel space generated by AMAPVox). Ray tracing is subsequently used to compute light availability at any location in the scene. Unless a particular LIDF is specified, the LIDF is assumed to be spherical (and to apply to all vegetation elements). In which case the transmittance is isotropic. Conversely, if a non-spherical LIDF is provided, the light attenuation will depend on the direction of the incoming light.

2.3.2.1. Pre-processing. We applied a 100 m buffer around the 4 hectares of the study, extending the study area to 16 ha, centred on the location of the microclimate sensors. This was done to avoid border effects and ensure that canopy conditions around the perimeter of each plot were captured, as forest gaps can modify understory microclimatic conditions tens of metres from the forest edge (Camargo and Kapos, 1995; Ewers and Banks-Leite, 2013). In the case of the UAV data, we used the ALS data as a buffer because the area scanned in UAV did not cover more than the 4 ha of interest.

2.3.2.2. Voxelization. In order to compute light extinction from multiple return pulses, we need to quantify individual return contributions to the extinction. Such information is not directly contained in the LiDAR data, but AMAPVox offers different alternatives to weight individual returns. A weight is given to each return to capture the unequal contribution of successive returns to the gradual extinction of a transmitted pulse. We used the apparent reflectance (i.e. reflected energy corrected for the distance dependent decay but not for unknown target reflectivity and orientation) as a proxy of this contribution (Yin et al., 2020). Because ground and vegetation reflectivity can differ significantly (Vincent et al., 2023), we first corrected ground reflectivity to match vegetation reflectivity by multiplying ground points' apparent reflectance by the ratio of the mean apparent reflectance of vegetation single returns to the mean apparent reflectance of ground single return.

In AMAPVox this apparent reflectance associated to each return is further normalised by dividing it by the sum of the apparent reflectance values of all returns from a given transmitted pulse.

The local attenuation of the laser light signal by the vegetation is then estimated from the optical path lengths - and return weights - of all incoming laser pulses in a 1 m^3 voxel. Various estimators of light attenuation are implemented in AMAPVox. They all make some regularity assumptions and notably assume random spatial distribution of leaves and branches within a voxel (no clumping). In the present study, we used the so-called Free Path Length estimator initially developed for single return scanners (Pimont et al., 2019) and later extended to multiple returns as described in Vincent et al. (2021). To study directional transmittance incoming pulses can be filtered by scanning angle range. By default, all incoming pulses are used, implicitly assuming that transmittance is isotropic.

In order to test the assumption of isotropic transmittance we also voxelized the drone data by angle sectors of 10° in size, ranging from 0° to 70° and tested if transmittance was dependent on lighting direction (See SI section *Anisotropy test*). The data used for this test were acquired on a one ha plot located in the same site with the same scanner and flight plan, but outside the 4-ha region of interest.

2.3.2.3. Dealing with locally low sampling. Thinning analyses showed that light attenuation estimation of voxels with less than 20 incoming pulses was positively biased. A small fraction of voxels (see SI Fig. S7 for the percentage of voxels poorly sampled along the canopy height gradient for the three LiDAR acquisitions) were not sufficiently sampled (or not sampled at all as could also occur due to occlusion). In that case light attenuation was estimated from a larger canopy volume centred on the target voxel. The target voxel was merged with the 26 nearest neighbouring voxels. In the rare case where the extended volume would still be sampled by too few pulses to get a reliable estimate, the median attenuation of the well-sampled voxels of the whole canopy was applied.

2.3.2.4. LAI2200 transmittance simulation from LiDAR. Based on the local light extinction rates estimated in a first step, AMAPVox can simulate LAI2200 acquisitions at the same X, Y, Z coordinates as the LAI2200 placed in the study area (described in section *LAI2200*). A ray-tracing algorithm is used to sample the same five angular sectors as the LAI2200. AMAPVox computes directional transmittance (default: 136 directions), then aggregates these values per ring, weighting each direction by its associated solid angle. No sky illumination model is applied.

The clearing in which the LAI2200 reference measurements were taken was not large enough to provide a field of view completely unobscured by vegetation. Indeed, the simulated transmittances obtained for rings 4 and 5 at the centre of the clearing were lower than 1 (resp. 0.96 and 0.23). Therefore, the average measured light level of the LAI2200 for rings 4 and 5 of the mobile LAI2200 unit was corrected by a multiplicative factor of 0.96 and 0.23 respectively prior to computing the ratio of below to above light level yielding the transmittance per ring.

2.3.2.5. Light maps (hemispherical transmittance with illumination model: Global Site Factor). AMAPVox also includes an option to generate light maps based on an insolation model. In this mode, it computes the Global Site Factor (GSF) on a grid — that is, the proportion of total (direct and diffuse) solar radiation received at a given location relative to the amount it would receive under open-sky conditions. Ray-tracing is used to predict light availability at any location in the scene. Individual rays reaching the location of interest from the hemisphere are weighted according to an insolation model which takes as input the plot location and orientation, the time period and the associated clearness index to integrate the direct and diffuse solar irradiance over time. Here the light is simulated at a latitude of 5° (French Guiana) for one year with an average clearness index (0.52) for the study period (from 01/04/2023 00:01 to 31/03/2024 23:59). The clearness index was computed from data of the Paracou flux tower as: *global solar irradiance/extraterrestrial radiation* (Liu and Jordan, 1960). The hemisphere was sampled in 136 directions. Multiple reflections are not considered in this simple model (see SI Fig. S5 right for an output transmittance map of the AMAPVox model).

2.3.3. Cross-validation of sensors data

We first controlled the coherence between the data acquired by the two field sensors (LAI2200 and HOBO) along the HOBO transect. For that we computed the Pearson's correlation between LAI2200 transmittances measures for the five rings and integrated over the rings, with the averaged light in lux measured over one year by the HOBO sensors. We also controlled the coherence of the spatial distribution of the light measured by the two field sensors, by plotting the light profiles in lux and transmittance on the HOBO transect, where the measurements were taken by the two sensors.

2.3.4. Comparison of LiDAR data to field validation data

2.3.4.1. Per individual sensor location. To compare transmittance estimated from different LiDAR acquisitions with transmittance measured by the LAI2200 sensor, for each point of measurement we averaged repeated readings and we computed Pearson's correlation coefficients and used multiple line plots.

2.3.4.2. Per inclination angle. To check the angular correctness of the estimated transmittance values, we compared the transmittance per ring simulated using the different LiDAR acquisitions with the values measured using the LAI2200 device.

2.3.4.3. Anisotropy effect in transmittance levels estimation. To test the effect of the angular distribution of leaves on the angular pattern of transmittance, we compared the Mean Relative Error (MRE) of the mean transmittance for both transects across the five rings (Eq. (1)) estimated with two different Leaf Inclination Distribution Functions (LIDF): spherical and plagiophile. Mean absolute error (MAE) (Eq. (2)) was also computed for each LIDF. Mean relative error provides a measure of the magnitude of the overall bias in transmittance (average error across all angular sectors). Mean absolute error provides a measure of the magnitude of the error per ring. Both errors are expressed relative to the mean measured transmittance.

$$\mathrm{MRE} = \frac{1}{5}\sum_{r}\frac{\frac{1}{n}\sum_{s} Est.\ transmittance_{r,s} - \frac{1}{n}\sum_{s} Obs.\ transmittance_{r,s}}{\frac{1}{n}\sum_{s} Obs.\ transmittance_{r,s}} \quad (1)$$

$$\mathrm{MAE} = \frac{1}{5}\sum_{r} \frac{\left| \frac{1}{n}\sum_{s} Est.\ transmittance_{r,s} - \frac{1}{n}\sum_{s} Obs.\ transmittance_{r,s} \right|}{\frac{1}{n}\sum_{s} Obs.\ transmittance_{r,s}} \quad (2)$$

With r = ring number (1 to 5), s = sensor number (1 to n, with n = number of measurement locations per transect).

2.3.5. Vertical forest structure heterogeneity

To check how variable is light availability vertically, and if ground-based sensors provide information about light availability further up in the canopy, we computed the Pearson's correlation of the hemispherical transmittances (light maps) between the lowest stratum and those above it. To check the spatial autocorrelation of vertical forest structure, we computed the Pearson's correlation between two consecutive forest strata over the whole vertical gradient.

3. Results

3.1. Cross-validation of sensors data

The Pearson's correlation values between the data acquired by the two field sensors (LAI2200 and HOBO) are reported in Fig. 1. LAI2200 light values are given as the transmittance (ratio between the measurement taken by the sensor placed below the forest canopy over the one taken in the reference open area). The HOBO sensor takes measurements in lux every 15 min, which are then averaged over one year for each sensor. The LAI2200 sensor measures light at five zenith solid angles, called rings, from 1 (most vertical) to 5 (most horizontal), at 20 measurement positions, with 4 replicates, for a total of 400 measurements. LAI2200_integrated is the weighted sum of the transmittances of the 5 rings measured by the LAI2200 sensors weighted by the solid angle of each ring. Readings are averaged over the four measurements repetitions, for each location. The HOBO annual light is strongly correlated with the LAI2200 light data integrated over the five rings (r = 0.98), which mainly represents the first three rings (ring 1: r = 0.93; ring 2: 0.95; ring 3: 0.79; ring 4: 0.53; ring 5: 0.52). Consistently, the first and the second rings of the LAI2200 light data

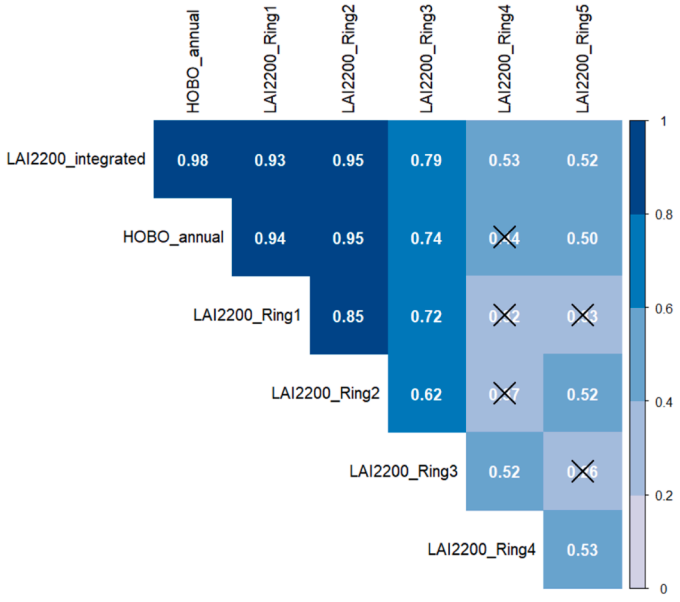

Fig. 1. Pearson's correlation matrix between LAI2200 and HOBO light measurements. The crosses indicate p-value > 0.05.

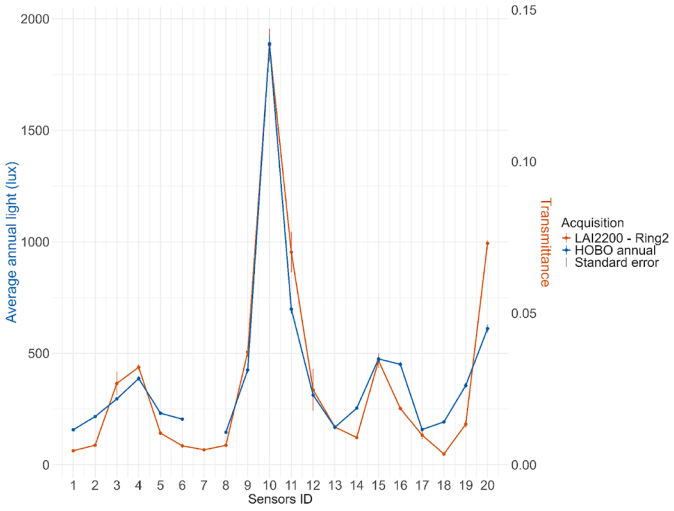

Fig. 2. Average annual light (in lux) acquired by the HOBO sensors and transmittance acquired in October (dry season) by LAI2200 sensor for ring 2 (the ring for which LAI2200 measurements were the most correlated with the HOBO measurements), on the HOBO transect. Note the different Y axes.

(expressed as transmittance) are highly correlated with the HOBO annual light data (in lux) (r = 0.94 and 0.95 respectively). The correlation is strong but less important for the third ring (r = 0.74), and moderate and barely significant for the last two rings (r = 0.44 and 0.5 respectively) (Fig. 1). The HOBO annual light is more correlated with the LAI2200 light data integrated over the five rings, than with the first three rings of the LAI2200 data taken separately (integrated: 0.98; ring 1: r = 0.94; ring 2: 0.95; ring 3: 0.74) (Fig. 1). A comparison of the spatial distribution of the light measured by the two field sensors shows that the HOBO spatial light profile is very close to the LAI2200 transmittance profiles of the second ring (Fig. 2).

3.2. Validation of LiDAR-derived LAI2200 light estimate

3.2.1. Per individual sensor location

The Pearson's correlation coefficients between the simulated LAI2200 values derived from the LiDAR acquisitions with the validation data (measured LAI2200 transmittances and average annual light in lux measured by HOBO) show a strong spatial consistency (r between 0.89 and 0.99 between LiDAR and LAI2200 for rings 1 and 2, between 0.92 and 0.98 between LiDAR and HOBO) (Table 3). For the two first rings,

Table 3
Pearson's correlations between light estimated from LiDAR (ALS high (1000 m) and low (500 m) altitude, and UAV) (in row) and light measured by field sensors (LAI2200, HOBO, in column) on HOBO transect only. Light is transmittance at the first and second ring (i.e. most vertical incident angles) in case of LAI2200 and LiDAR and is in lux averaged over the year in case of HOBO. LiDAR transmittance is estimated at 1 m resolution. All the p-values are < 0.0001. See SI Table S3 for all the Pearson's correlations.

	HOBO annual	LAI2200 ring 1	LAI2200 ring 2
ALS low altitude ring 1	0.94	0.99	–
ALS low altitude ring 2	0.98	–	0.94
UAV ring 1	0.92	0.99	–
UAV ring 2	0.97	–	0.92
ALS high altitude ring 1	0.92	0.98	–
ALS high altitude ring 2	0.95	–	0.89

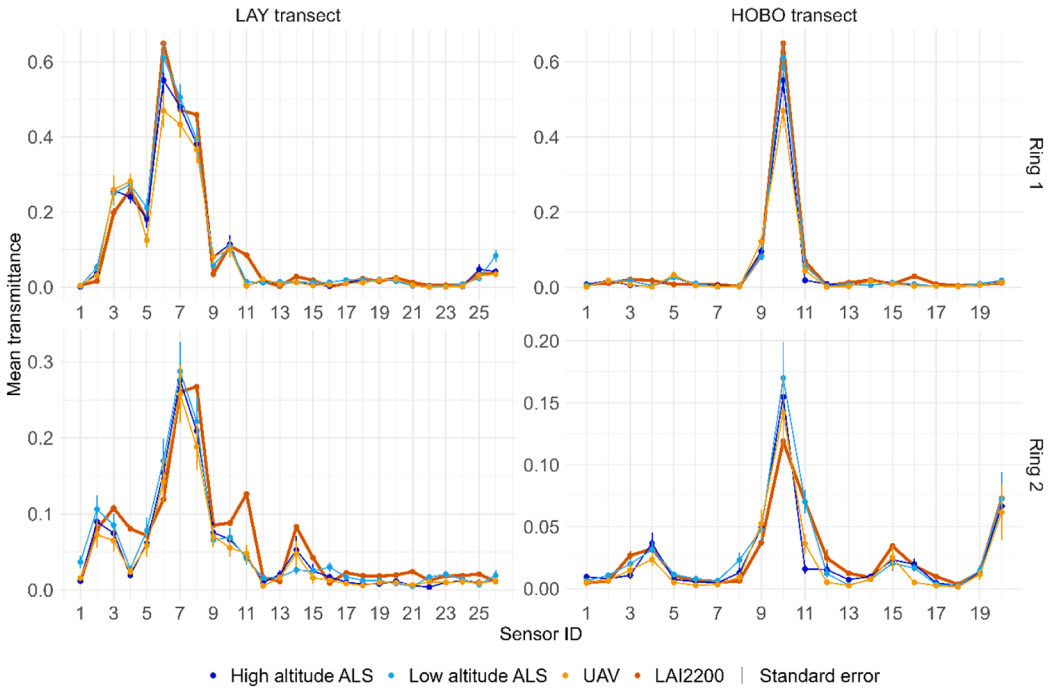

Fig. 3. Average transmittances of the first (top) and the second ring (bottom) measured by LAI2200 and estimated from each LiDAR acquisition at each sensor location of the LAY (left) and HOBO transects (right). LiDAR transmittance is estimated at 1 m resolution. Note the y-axis differences in scale. See SI Fig. S6 for the other rings.

Table 4
Pearson's correlations between light (transmittance) estimated from LiDAR (ALS high (1000 m) and low (500 m) altitude, and UAV) and measured by field sensors (LAI2200) on both transects (LAY and HOBO) at the first and second ring (i.e. incident angle). LiDAR transmittance is estimated at 1 m resolution. All the p-values are < 0.001. See SI Table S4 for all the Pearson's correlations.

	LAI2200 ring 1	LAI2200 ring 2
ALS low altitude ring 1	0.99	–
ALS low altitude ring 2	–	0.92
ALS high altitude ring 1	0.98	–
ALS high altitude ring 2	–	0.93
UAV ring 1	0.97	–
UAV ring 2	–	0.94

the spatial transmittance profiles of the LiDAR follow the spatial transmittance profile of the LAI2200 well, except for sensor 11 on the LAY transect (Fig. 3). The HOBO data are more correlated with the transmittances of the second ring of the LiDAR than with the first ring, as was the case with the LAI2200 rings (Table 3; Fig. 1). We can also see that the HOBO spatial light profile is very close to the LAI2200 and LiDAR transmittance profiles of the second ring (Figs. 2, 3 bottom right). On the HOBO transect, the HOBO and the LAI2200 data have the highest correlations with the low altitude ALS (r = 0.98 and 0.99 respectively), followed by the UAV (r = 0.97 and 0.99 respectively) and the high altitude ALS (r = 0.95 and 0.98 respectively) (Table 3). Considering both transects, for the first ring the low altitude ALS has the highest

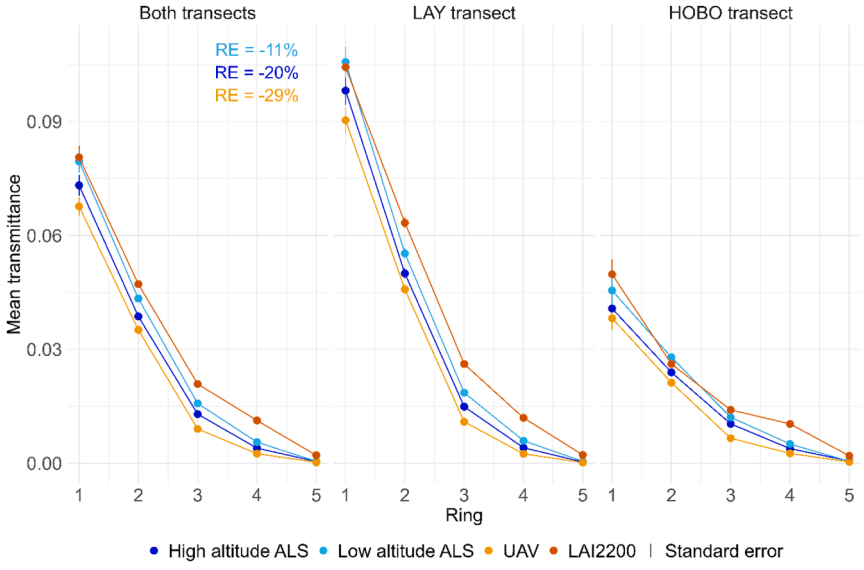

Fig. 4. Average transmittances measured by LAI2200 and estimated from each LiDAR acquisition of the two transects (left), and of the LAY (centre) and HOBO transects (right), at five incident angles (rings). Mean Relative Error (MRE) in percent is given for each LiDAR acquisition. LiDAR transmittance is estimated at 1 m resolution.

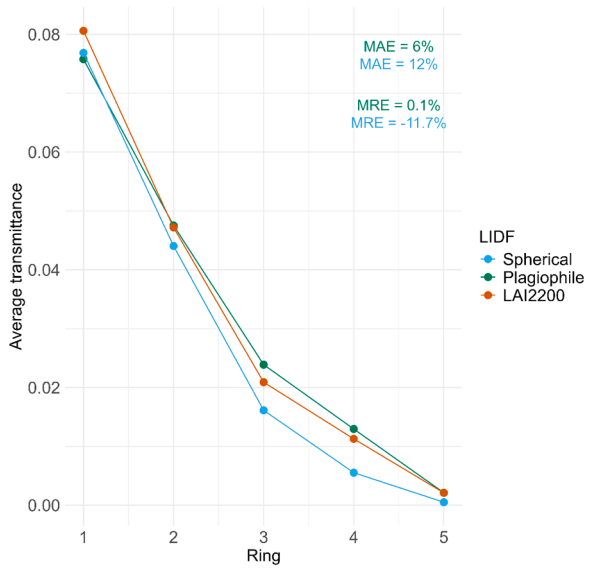

Fig. 5. Average transmittance for both transects, measured by LAI2200 and estimated from low altitude ALS with two different Leaf Inclination Distribution Functions (LIDF): spherical and plagiophile, at five viewing angles (rings). Mean absolute error (MAE) and mean relative error (MRE) in percent are given for each LIDF.

correlations with the LAI2200 data ($r = 0.99$), followed by the high altitude ALS ($r = 0.98$) and the UAV ($r = 0.97$) (Table 4). On the spatial light profiles of the first ring, the values of the low altitude ALS are closer to the LAI2200 values than the high altitude ALS and the UAV (Fig. 3).

3.2.2. Per inclination angle

To assess the ability to estimate the angular distribution of light, we compared light estimated by radiative transfer from LiDAR data and that measured by LAI2200, averaged over all locations of a transect for the different solid angles (rings). The average angular transmittance profiles of the LiDAR follow well the average angular transmittance profile of the LAI2200 (Fig. 4). The smallest relative error is 11 % recorded by the low altitude ALS, the largest is 29 % recorded by the UAV. For all rings, the values of the low altitude ALS are closer to the LAI2200 values followed by the high altitude ALS and the UAV (Fig. 4).

Consideration of a plagiophile function of leaf inclination compared to a spherical function halves the normalised mean absolute error of the transmittance estimation from the low altitude ALS ($ME_{plagiophile} = 6$ %, $ME_{spherical} = 12$ %) and strongly reduces the relative mean error ($RE_{plagiophile} = 0.1$ %, $RE_{spherical} = -11.7$ %) (Fig. 5).

3.3. Vertical forest structure heterogeneity

We studied the variation of light levels as hemispherical transmittances along the vertical gradient of the canopy, and its spatial autocorrelation along the vertical axis. The correlation between the horizontal spatial distribution of the hemispherical transmittances of the lowest stratum and that of a stratum above steadily decreases when the distance between the above stratum and the first stratum increases (Fig. 6 left). The horizontal spatial distribution of the hemispherical transmittances of the first and the last strata of the forest are not correlated ($r = 0.02$) (Fig. 6 left). Consecutive forest strata are less and less correlated with each other as they are located higher in the canopy ($r = 0.8$ between the two first strata, $r = 0.6$ between the two last strata from the ground) (Fig. 6 right).

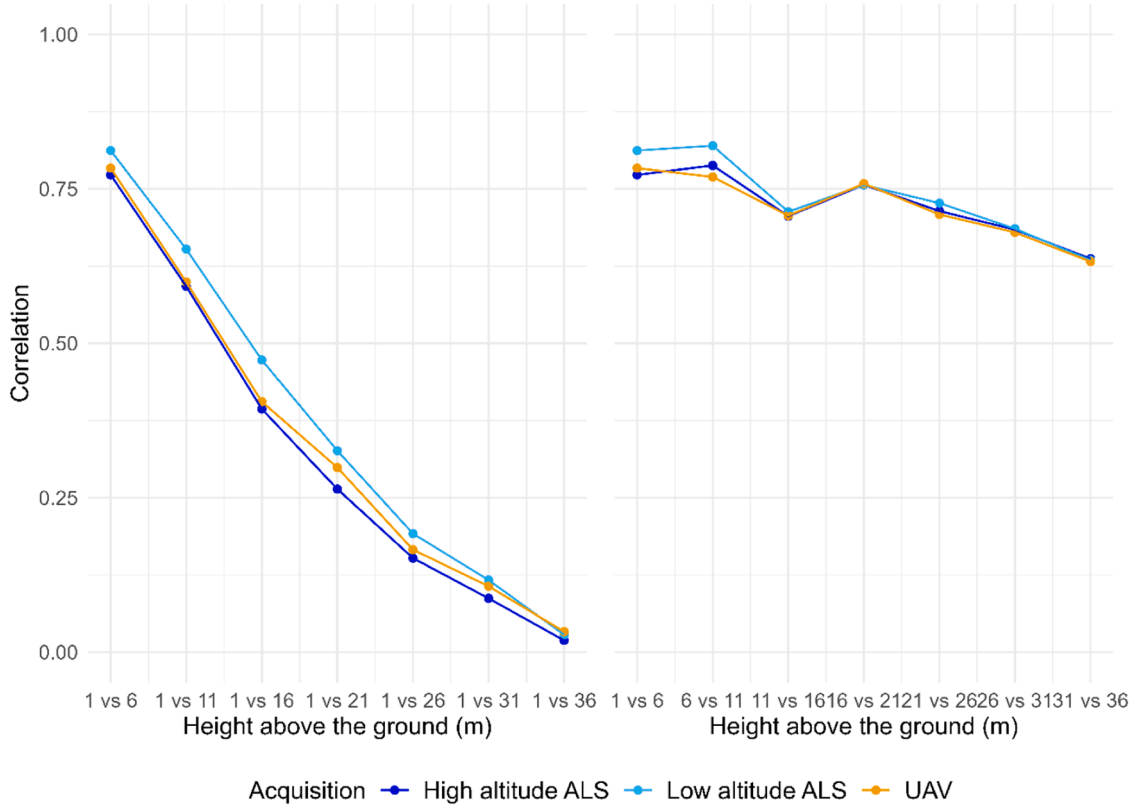

Fig. 6. Pearson's correlation of the horizontal spatial distribution of the hemispherical transmittances (light maps) between the lowest stratum and those above it (left) and between two consecutive forest strata (right), for each LiDAR acquisition. The transmittance is computed on a grid, every 10 m horizontally and every 5 m vertically.

4. Discussion

We used field-based measurements of environmental conditions as ground-truthing to compare three different methods of LiDAR acquisition. These were a high density ALS, a more penetrating ALS, and a denser UAV, and we compared their ability to characterise the understory light environment in a dense tropical rainforest. To this aim we tested LiDAR ability to estimate the spatial and angular variation of light in a tropical forest understory. Finally, we studied the vertical variability of light to determine to what extent ground-based sensors may inform on light higher up in the canopy. Our results show that the vertical structure of the forest is very heterogeneous, and the light level in the upper canopy is not indicative of the light level of the understory. This means that sensors placed in the understory cannot be used to describe the light at the top of the canopy. LiDAR was shown to be very effective to characterise the forest light environment, including the understory, in a spatially and angularly consistent way. Among the LiDARs used in this study, (i) a low altitude ALS (500 m) can better describe the understory canopy structure and thus the understory microenvironment, thanks to its higher penetration; (ii) Despite its very high sampling intensity, UAV LiDAR is the acquisition that most underestimates light levels. We demonstrated that taking into account the anisotropic nature of light transmittance improved the estimation of absolute light levels by radiative transfer.

4.1. Cross-validation of sensors data

Measurements of both field sensors show good agreement for the two innermost rings recorded by the LAI2200 sensor. In contrast transmittance measurements at outer zenith angles (rings 4 and 5) are generally less informative and more prone to noise than those at lower angles. This limitation is reflected in our data: the variability in HOBO light sensor readings appears to be primarily influenced by incoming light at inner zenith angles (rings 1 and 2). These rings show the highest correlation with HOBO measurements, as illustrated in Fig. 1. In contrast, rings 4 and 5 show much lower and barely significant correlations. Modelled transmittance per ring from LiDAR data, also shows lower correlation with LAI2200 measurements for outer rings, further indicating a degradation of signal-to-noise ratio (SNR) as shown in Fig. S6. This likely results from both a reduction in the absolute light levels reaching the sensor under dense canopy (due to longer optical paths inside the canopy at lower elevation angles) and a reduced relative variability, as outer rings integrate light over increasingly large sectors of the sky (see Table 1).

4.2. Comparison of the performance of different LiDAR acquisitions

The LAI2200 data simulated by LiDAR are highly coherent with the validation data for rings 1 and 2, and the spatial distribution of transmittance described by LiDAR is consistent with that measured by LAI2200 for the most vertical rings (Table 3; Fig. 3; See SI Fig. S6 for results of the other rings). The angular light distribution estimated from LiDAR is less consistent, showing a tendency to underestimate light levels measured by LAI2200 at low inclination angles, which nevertheless contribute little to total transmittance (Fig. 4). Considering both transects, the low altitude ALS is the acquisition that better describes the light environment at 1 m height, followed by the high altitude ALS and then the UAV (Table 4). Transmittances per incident angle estimated from LiDAR data are closer to the measured data when acquired with low altitude ALS, followed by high altitude ALS and then UAV (Fig. 4). That can be explained by the limited sensitivity of the UAV LiDAR sensor which leads to an overestimation of the absorbance: some of the laser light is reflected with an intensity too low to be detectable, leading to underestimating the transmittance.

UAV and high altitude ALS have a higher sampling intensity than low altitude ALS. The density of the point cloud acquired is greatest for UAV acquisition (2600 points/m^2), and ALS high altitude acquisition is also denser (350 points/m^2) than ALS low altitude acquisition (50 points/m^2) (Table 1: Characteristics of LiDAR acquisitions; See SI Fig. S7 for the percentage of voxels poorly sampled along the canopy height gradient, for the three LiDAR acquisitions). On the other hand, low altitude ALS has a higher penetration rate (19 % of shots reach the ground) than the high altitude ALS (10 %), and the UAV has the lowest (4 %). Thanks to its higher penetration rate compared to the high altitude ALS and the UAV, low altitude ALS can better describe the entire canopy profile, explaining the relative performance of these three acquisitions. These results show that high pulse density does not guarantee an accurate characterization of the forest structure through the entire profile, including the understory, and that penetration rate is of major importance. This result is consistent with Vincent et al. (2023) which reported that irradiance at canopy level and sensitivity of the laser system strongly affected the detectability of vegetation elements and completeness of the vertical profile.

4.3. Importance of light transmittance anisotropy

The major source of discrepancy between modelled and measured light levels occurs at low light incident angles (Fig. 4; SI Fig. S6). This is likely due to our assumption of light transmittance being independent of light incidence angle (isotropic). This is a hypothesis often made for simplicity (see section reviewing existing forest light models in *Introduction*) but probably rarely met. We specifically tested that assumption by voxelizing the UAV data which has a much larger swath angle than standard ALS scanners, by angular sectors of 10° in size, ranging from 0° to 70°. We found a highly significant dependency of light attenuation on light incidence angle, which decreased as incident angle was less vertical (See SI section *Anisotropy test*). As a consequence, considering a plagiophile leaf inclination angle when computing transmittance provided a better fit of simulated transmittance level across LAI2200 rings, compared to a spherical function (Fig. 5). For a more accurate estimate of absolute light levels, a more detailed study of the variation in the angular distribution of leaves in space is required.

4.4. Limits

Slight variation in the position of sensors have been reported to result in large changes in recorded light or temperature (Bramer et al., 2018; Zellweger et al., 2019b). Geolocation inaccuracies of sensors may explain local discrepancies between modelled and measured light levels (such as for sensor 11 of the LAY transect, Fig. 3 top). By optimising the sensor coordinates to reduce the difference between the transmittance measured and predicted by LiDAR (see SI section *Sensors coordinates optimisation*, Fig. S8) the error was reduced by up to 0.03 (95 % quantile) and the median displacement was −0.5 m in x (range: −1.0; 1.0), 0 m in y (range: −1.0; 1.0). Optimized coordinates were not used in this study as this might have led to overfitting. Change in the local environment (due for instance to a fallen or displaced branch) between the measurement's dates of LAI2200 and LiDAR (21, 22 and 25/10/2023 for the LAI2200, and 19 and 26/10/2023 for the LiDAR) may also play a role in the observed discrepancies.

4.5. Recommendations

To characterise the light environment at any point in a forest, we recommend using a LiDAR able to accurately sample the entire forest structure at all azimuth angles, i.e. with a high penetration rate and wide scan angles). None of the three LiDAR acquisitions tested in this study combined both characteristics. The combination of wide swath and high penetration may only be available in high-end UAV systems such as the Riegl VUX1-LR (https://www.rieglusa.com/wp-content/uploads/vux-1lr-datasheet.pdf) which is also much heavier and costly than the ultra lightweight LiDAR used here. The choice of LiDAR and acquisition

characteristics will also depend on the area to study, the temporal resolution of interest, access to calibration data and the available budget. With a low budget and an interest in frequent acquisitions (Anderson and Gaston, 2013) and studying the anisotropic nature of light, the UAV is the most interesting acquisition mode, but requires calibration data to correct for its underestimation of light levels. For a better characterisation of the understory by aerial LiDAR acquisition, a high power and low altitude ALS is more suitable as both characteristics contribute to increasing the penetration and to better describing the canopy profile. However, both characteristics will require closer flight lines and longer flight times to reach equivalent sampling density. This is because higher power implies lower Pulse Repetition Rate and lower flight height reduces effective sampling area. Another possibility is to combine ground and above canopy measurements to avoid any potential occlusion (Schneider et al., 2019). However, there are still a number of issues to be dealt with before being able to effectively apply ray-tracing analysis to terrestrial MLS (Mobile Laser Scanning) data. First, the optical paths of non-intercepted pulses have to be reconstructed from the scanning characteristics and trajectory. This is only partially addressed in (Che and Olsen, 2019) and the proposed solution is not openly available. Second, true misses (no-hit pulses) have to be distinguished from hits occurring before the minimum detection range (typically between 0.5 and 1 m). Third, as is the case for TLS, partial hits will introduce additional uncertainty (Kent and Bailey, 2024) which needs further consideration.

4.6. Conclusion

We have shown that (i) Aerial LiDAR which provides an accurate description of forest structure can effectively characterise the forest light environment even in a highly diverse dense tall forest. It does not rely upon largely unavailable species-specific information. It represents an improvement over ground measurement with light sensors, because the light at ground level is not representative of the light level prevailing in the upper canopy; (ii) LiDAR can be used to estimate the light environment in the understory in a spatially and angularly consistent way; (iii) high pulse density does not guarantee an accurate characterization of the forest structure, and high penetration rate is critical to accurately describe the forest structure, including the understory; (iv) the anisotropic nature of light transmittance should be taken into account in the estimation of absolute light levels.

Using remote sensing to estimate the microenvironment improves our mechanistic understanding of how vegetation structure determines microclimate. LiDAR data can improve habitat suitability maps and predictions of species response to change in canopy structure (Zellweger et al., 2019a; De Frenne, 2024). Using detailed micro-environment data in species distribution models will allow more individual-centred approaches to determine species range limits and their evolution related to climate change (Zellweger et al., 2020; Lembrechts et al., 2019). For forest managers and nature conservationists micro-environment monitoring and mapping help to manage natural resources efficiently as it allows to (i) optimise regeneration or planting in accordance to tree species-specific light resource needs (Aussenac, 2000), (ii) adapt harvesting choices (selective logging, liberation thinning, gaps size) (Hai et al., 2023), (iii) adapt ecosystems to stand management and climate change in increasing structural heterogeneity by promoting tree size diversity (Ehbrecht et al., 2019; Beugnon et al., 2024) and (iv) identify habitats of rare or threatened species that need protection.

CRediT authorship contribution statement

Vincyane Badouard: Writing – review & editing, Writing – original draft, Visualization, Validation, Resources, Project administration, Methodology, Funding acquisition, Formal analysis, Data curation, Conceptualization. **Philippe Verley:** Writing – review & editing, Software, Methodology. **Yuchen Bai:** Writing – review & editing, Resources, Methodology, Formal analysis, Data curation. **Giacomo Sellan:** Writing – review & editing, Resources. **Léa Françoise:** Writing – review & editing, Resources. **Eric Marcon:** Writing – review & editing, Validation, Supervision, Resources, Project administration, Methodology, Funding acquisition. **Géraldine Derroire:** Writing – review & editing, Validation, Supervision, Resources, Project administration, Methodology, Funding acquisition. **Grégoire Vincent:** Writing – review & editing, Validation, Supervision, Resources, Project administration, Methodology, Investigation, Funding acquisition, Conceptualization.

Declaration of competing interest

The authors declare the following financial interests/personal relationships which may be considered as potential competing interests:

Vincyane Badouard reports financial support was provided by French National Research Agency. If there are other authors, they declare that they have no known competing financial interests or personal relationships that could have appeared to influence the work reported in this paper.

Acknowledgments

This work has benefited from support of a grant from Investissement d'Avenir grants of the ANR (CEBA: ANR-10-LABX-25-01) and a grant managed by the Agence Nationale de la Recherche (AIBSI: ANR-22-EXES-0005), as part of the France 2030 program. It was also supported by the University of French Guiana and the Ministère Français de l'Enseignement Supérieur et de la Recherche. We thank the Paracou research field station in French Guiana managed and supported by CIRAD, UMR EcoFoG (https://paracou.cirad.fr), which benefits from "Investissement d'Avenir" grants managed by Agence Nationale de la Recherche (AnaEE France ANR-11-INBS-0001; Labex CEBA ANR-10-LABX-25-01). We thank Benoit Burban for piloting the drone, and Giovanni Frati for taking time to share his LiDAR expertise with the first author and for proofreading the article.

Supplementary materials

Supplementary material associated with this article can be found, in the online version, at doi:10.1016/j.agrformet.2025.110713.

Data availability

Data will be made available on request.

References

Anderson, K., Gaston, K.J., 2013. Lightweight unmanned aerial vehicles will revolutionize spatial ecology. Front. Ecol. Environ. 11 (3), 138–146. https://doi.org/10.1890/120150.

Atkins, J.W., Fahey, R.T., Hardiman, B.H., Gough, C.M., 2018. Forest canopy structural complexity and light absorption relationships at the subcontinental scale. J. Geophys. Res. Biogeosci. 123 (4), 1387–1405. https://doi.org/10.1002/2017JG004256.

Aubry-Kientz, M., Dutrieux, R., Ferraz, A., Saatchi, S., Hamraz, H., Williams, J., Coomes, D., Piboule, A., Vincent, G., 2019. A comparative assessment of the performance of individual tree crowns delineation algorithms from ALS data in tropical forests. Remote Sens. 11 (9), 1086. https://doi.org/10.3390/rs11091086.

Aussenac, G., 2000. Interactions between forest stands and microclimate: ecophysiological aspects and consequences for silviculture. Ann. For. Sci. 57 (3), 287–301. https://doi.org/10.1051/forest:2000119.

Baraloto, C., Couteron, P., 2010. Fine-scale microhabitat heterogeneity in a French Guianan forest. Biotropica 42 (4), 420–428. https://doi.org/10.1111/j.1744-7429.2009.00620.x.

Bauwens, S., Bartholomeus, H., Calders, K., Lejeune, P., 2016. Forest inventory with terrestrial LiDAR: a comparison of static and hand-held mobile laser scanning. Forests 7 (6), 127. https://doi.org/10.3390/f7060127.

Becker, P., Erhart, D.W., Smith, A.P., 1989. Analysis of forest light environments part I. computerized estimation of solar radiation from hemispherical canopy photographs. Agric. For. Meteorol. 44 (3–4), 217–232. https://doi.org/10.1016/0168-1923(89)90018-X.

Berezowski, T., Kośmider, J., Greczuk, M., Chormański, J., 2015. LAI variability as a habitat feature determining reptile occurrence: a case study in large forest complexes in Eastern Poland. Forests 6 (4), 957–972. https://doi.org/10.3390/f6040957.

Beugnon, R., Le Guyader, N., Milcu, A., Lenoir, J., Puissant, J., Morin, X., Hättenschwiler, S., 2024. Microclimate modulation: an overlooked mechanism influencing the impact of plant diversity on ecosystem functioning. Glob. Change Biol. 30 (3), e17214. https://doi.org/10.1111/gcb.17214.

Bramer, I., Anderson, B.J., Bennie, J., Bladon, A.J., De Frenne, P., Hemming, D., Hill, R. A., Kearney, M.R., Körner, C., Korstjens, A.H., Lenoir, J., Maclean, I.M.D., Marsh, C. D., Morecroft, M.D., Ohlemüller, R., Slater, H.D., Suggitt, A.J., Zellweger, F., Gillingham, P.K., 2018. Advances in monitoring and modelling climate at ecologically relevant scales. Adv. Ecol. Res. 101–161. https://doi.org/10.1016/bs.aecr.2017.12.005. Vol. 58,Academic Press Inc.

Brede, B., Bartholomeus, H.M., Barbier, N., Pimont, F., Vincent, G., Herold, M., 2022. Peering through the thicket: effects of UAV LiDAR scanner settings and flight planning on canopy volume discovery. Int. J. Appl. Earth Observ. Geoinf. 114, 103056. https://doi.org/10.1016/j.jag.2022.103056.

Camargo, J.L.C., Kapos, V., 1995. Complex edge effects on soil moisture and microclimate in central Amazonian forest. J. Trop. Ecol. 11 (2), 205–221. https://doi.org/10.1017/S026646740000866X.

Chazdon, R.L., Field, C.B., 1987. Photographic estimation of photosynthetically active radiation: evaluation of a computerized technique. Oecologia 73, 525–532. https://doi.org/10.1007/BF00379411.

Che, E., Olsen, M.J., 2019. An efficient framework for mobile lidar trajectory reconstruction and Mo-norvana segmentation. Remote Sens. 11 (7), 836. https://doi.org/10.3390/RS11070836.

Clements, F.E., 1916. Plant Succession: an Analysis of the Development of Vegetation. Carnegie institution of Washington. http://www.archive.org/cletails/cu31924000531818.

Collinet, F. (1997). *Essai de regroupements des principales espèces structurantes d'une forêt dense humide d'après l'analyse de leur répartition spatiale (Forêt de Paracou-Guyane)* (Doctoral dissertation, Université Claude Bernard Lyon 1).1-301.

De Frenne, P., 2024. Novel light regimes in European forests. Nat. Ecol. Evol. 8 (2), 196–202. https://doi.org/10.1038/s41559-023-02242-2.

Denslow, J.S., Gomez Diaz, A.E., 1990. Seed rain to tree-fall gaps in a neotropical rain forest. Can. J. For. Res. 20 (5), 642–648. https://doi.org/10.1139/x90-086.

Ehbrecht, M., Schall, P., Ammer, C., Fischer, M., Seidel, D., 2019. Effects of structural heterogeneity on the diurnal temperature range in temperate forest ecosystems. For. Ecol. Manag. 432, 860–867. https://doi.org/10.1016/j.foreco.2018.10.008.

Endler, J.A., 1993. The color of light in forests and its implications. Ecol. Monogr. 63 (1), 1–27. https://doi.org/10.2307/2937121.

Engelbrecht, B.M.J., Herz, H.M., 2001. Evaluation of different methods to estimate understorey light conditions in tropical forests. J. Trop. Ecol. 17 (2), 207–224. https://doi.org/10.1017/S0266467401001146.

Ewers, R.M., Banks-Leite, C., 2013. Fragmentation impairs the microclimate buffering effect of tropical forests. PLoS One 8 (3), e58093. https://doi.org/10.1371/journal.pone.0058093.

Ferment, A., Picard, N., Gourlet-Fleury, S., Baraloto, C., 2001. A comparison of five indirect methods for characterizing the light environment in a tropical forest. Ann. For. Sci. 58 (8), 877–891. https://doi.org/10.1051/forest:2001171.

Finegan, B., 1996. Pattern and process in neotropical secondary rain forests: the first 100 years of succession. Trends Ecol. Evol. 119–124. https://doi.org/10.1016/0169-5347(96)81090-1. Vol. 11, Issue 3Elsevier Ltd.

Fortunel, C., Paine, C.E.T., Fine, P.V.A., Mesones, I., Goret, J.Y., Burban, B., Cazal, J., Baraloto, C., 2016. There's no place like home : seedling mortality contributes to the habitat specialisation of tree species across Amazonia. Ecol. Lett. 19, 1256–1266. https://doi.org/10.1111/ele.12661.

Gaquière, T., 2024. Dynamique de trouées de forêts naturelles et exploitées, applications à la régénération d'espèces exploitées En Guyane. Université de Guyane, pp. 1–138.

Gastellu-Etchegorry, J.P., Yin, T., Lauret, N., Grau, E., Rubio, J., Cook, B.D., Morton, D. C., Sun, G., 2016. Simulation of satellite, airborne and terrestrial LiDAR with DART (I): waveform simulation with quasi-Monte Carlo ray tracing. Remote Sens. Environ. 184, 418–435. https://doi.org/10.1016/j.rse.2016.07.010.

Goulamoussène, Y., Bedeau, C., Descroix, L., Linguet, L., Hérault, B., 2017. Environmental control of natural gap size distribution in tropical forests. Biogeosciences 14 (2), 353–364. https://doi.org/10.5194/bg-14-353-2017.

Hai, N.H., Phomphoumy, K., Quy, N.V., 2023. Nearest neighbor patterns of dominant tree species in tropical forests, Phou Khao Khouay National Park, Laos. J. For. Sci. Technol. 15, 16–26. https://doi.org/10.55250/jo.vnuf.2023.15.016-026.

Halverson, M.A., Skelly, D.K., Kiesecker, J.M., Freidenburg, L.K., 2003. Forest mediated light regime linked to amphibian distribution and performance. Oecologia 134 (3), 360–364. https://doi.org/10.1007/s00442-002-1136-9.

Hovi, A., Janoutová, R., Malenovský, Z., Schraik, D., Gastellu-Etchegorry, J., Lauret, N., Novotný, J., Rautiainen, M., 2024. Physically based modelling of spectral transmittance through forest canopies. Methods Ecol. Evol. 15 (10), 1859–1872. https://doi.org/10.1111/2041-210X.14402.

Huertas, C., Sabatier, D., Derroire, G., Ferry, B., Jackson, T.D., Pélissier, R., Vincent, G., 2022. Mapping tree mortality rate in a tropical moist forest using multi-temporal LiDAR. Int. J. Appl. Earth Observ. Geoinf. 109 (102780), 1–15. https://doi.org/10.1016/j.jag.2022.102780.

Jucker, T., Hardwick, S.R., Both, S., Elias, D.M.O., Ewers, R.M., Milodowski, D.T., Swinfield, T., Coomes, D.A., 2018. Canopy structure and topography jointly constrain the microclimate of human-modified tropical landscapes. Glob. Change Biol. 24 (11), 5243–5258. https://doi.org/10.1111/gcb.14415.

Kent, E.R., Bailey, B.N., 2024. Does intensity-based weighting of multiple-return terrestrial LiDAR data improve leaf area density estimates? Remote Sens. Environ. 311, 114229. https://doi.org/10.1016/j.rse.2024.114229.

Laurans, M., 2013. Rôle de la lumière dans la coexistence des espèces d'arbres de forêt tropicale humide : analyse des variations inter- et intra-spécifiques des performances et des traits fonctionnels. [Doctoral dissertation, Montpellier SupAgro]. 1-106 In Archives Ouvertes. https://tel.archives-ouvertes.fr/tel-01076209.

Laurans, M., Hérault, B., Vieilledent, G., Vincent, G., 2014. Vertical stratification reduces competition for light in dense tropical forests. For. Ecol. Manag. 329, 79–88. https://doi.org/10.1016/j.foreco.2014.05.059.

Lee, C.-C., Wang, C.-K., 2013. October). LiDAR penetration comparison at different altitudes and scanning angles in subtropical forest. Silvilaser, Beijing, China. https://www.researchgate.net/publication/327079124.

Lembrechts, J.J., Nijs, I., Lenoir, J., 2019. Incorporating microclimate into species distribution models. Ecography 42 (7), 1267–1279. https://doi.org/10.1111/ecog.03947.

Lenoir, J., Hattab, T., Pierre, G., 2017. Climatic microrefugia under anthropogenic climate change: implications for species redistribution. Ecography 40 (2), 253–266. https://doi.org/10.1111/ecog.02788.

Liu, B.Y.H., Jordan, R.C., 1960. The interrelationship and characteristic distribution of direct, diffuse and total solar radiation. Sol. Energy 4 (3), 1–19. https://doi.org/10.1016/0038-092X(60)90062-1.

Moeser, D., Roubinek, J., Schleppi, P., Morsdorf, F., Jonas, T., 2014. Canopy closure, LAI and radiation transfer from airborne LiDAR synthetic images. Agric. For. Meteorol. 197, 158–168. https://doi.org/10.1016/j.agrformet.2014.06.008.

Myneni, R.B., Ross, J., 1989. A review on the theory of photon transport in leaf canopies. Agric. For. Meteorol. 45 (1), 1–153. https://doi.org/10.1016/0168-1923(89)90002-6.

Næsset, E., Jonmeister, T., 2002. Assessing point accuracy of DGPS under forest canopy before data acquisition, in the field and after postprocessing. Scand. J. For. Res. 17 (4), 351–358. https://doi.org/10.1080/02827580260138099.

Nagata, M., Yamamoto, N., Shigeyama, T., Terasawa, Y., Anai, T., Sakai, T., Inada, S., Arima, S., Hashiguchi, M., Akashi, R., Nakayama, H., Ueno, D., Hirsch, A.M., Suzuki, A., 2015. Red/far Red light controls arbuscular mycorrhizal colonization via jasmonic acid and strigolactone signaling. Plant Cell Physiol. 56 (11), 2100–2109. https://doi.org/10.1093/pcp/pcv135.

Nicotra, A.B., Chazdon, R.L., Iriarte, S.V.B., 1999. Spatial heterogeneity of light and woody seedling regeneration in tropical wet forests. Ecology 80 (6), 1908–1926. https://doi.org/10.1890/0012-9658(1999)080[1908:SHOLAW]2.0.CO;2.

Nyman, P., Metzen, D., Hawthorne, S.N.D., Duff, T.J., Inbar, A., Lane, P.N.J., Sheridan, G.J., 2017. Evaluating models of shortwave radiation below eucalyptus canopies in SE Australia. Agric. For. Meteorol. 246, 51–63. https://doi.org/10.1016/j.agrformet.2017.05.025.

Peng, S., Zhao, C., Xu, Z., 2014. Modeling spatiotemporal patterns of understory light intensity using airborne laser scanner (LiDAR). ISPRS J. Photogramm. Remote Sens. 97 (July), 195–203. https://doi.org/10.1016/j.isprsjprs.2014.09.003.

Pimont, F., Soma, M., Dupuy, J.L., 2019. Accounting for wood, foliage properties, and laser effective footprint in estimations of leaf area density from multiview-LiDAR data. Remote Sens. 11 (13), 1580. https://doi.org/10.3390/rs11131580.

Pisek, J., Sonnentag, O., Richardson, A.D., Mõttus, M., 2013. Is the spherical leaf inclination angle distribution a valid assumption for temperate and boreal broadleaf tree species? Agric. For. Meteorol. 169, 186–194. https://doi.org/10.1016/j.agrformet.2012.10.011.

Poorter, L., Arets, E.J.M.M., 2003. Light environment and tree strategies in a Bolivian tropical moist forest: an evaluation of the light partitioning hypothesis. Plant Ecol. 166 (2), 295–306. https://doi.org/10.1023/A:1023295806147.

Purfürst, T., 2022. Evaluation of static autonomous GNSS positioning accuracy using single-, dual-, and tri-frequency smartphones in forest canopy environments. Sensors 22 (3), 1289. https://doi.org/10.3390/s22031289.

Roussel, J.R., Auty, D., Coops, N.C., Tompalski, P., Goodbody, T.R.H., Meador, A.S., Bourdon, J.F., de Boissieu, F., Achim, A., 2020. lidR: an R package for analysis of Airborne Laser Scanning (ALS) data. Remote Sens. Environ. 251, 112061. https://doi.org/10.1016/j.rse.2020.112061.

Osunkoya, O.O., 1992. Ecology of seed survival and seedling establishment in Australian tropical Rainforest. The Australian National University, pp. 1–176. https://doi.org/10.25911/5d6f9af1a8b76.

Roussel, J.-R., Auty, D., De Boissieu, F., & Meador, A.S. (2024). Package 'lidR'. https://cran.gedik.edu.tr/web/packages/lidR/lidR.pdf.

Scanga, S.E., 2014. Population dynamics in canopy gaps: nonlinear response to variable light regimes by an understory plant. Plant Ecol. 215 (8), 927–935. https://doi.org/10.1007/s11258-014-0344-9.

Schneider, F.D., Kükenbrink, D., Schaepman, M.E., Schimel, D.S., Morsdorf, F., 2019. Quantifying 3D structure and occlusion in dense tropical and temperate forests using close-range LiDAR. Agric. For. Meteorol. 268, 249–257. https://doi.org/10.1016/j.agrformet.2019.01.033.

Shirley, H.L., 1929. The influence of light intensity and light quality upon the growth of plants. Am. J. Bot. 16 (5), 354–390.

Tao, S., Labrière, N., Calders, K., Fischer, F.J., Rau, E.P., Plaisance, L., Chave, J., 2021. Mapping tropical forest trees across large areas with lightweight cost-effective terrestrial laser scanning. Ann. For. Sci. 78 (4), 103. https://doi.org/10.1007/s13595-021-01113-9.

Terborgh, J., 1985. The vertical component of plant species diversity in temperate and tropical forests. Am. Nat. 126 (6), 760–776. https://www.jstor.org/stable/2461255.

Théry, M., 2001. Forest light and its influence on habitat selection. Plant Ecol. 153 (1–2), 251–261. https://doi.org/10.1023/A:1017592631542.

Thom, D., Sommerfeld, A., Sebald, J., Hagge, J., Müller, J., Seidl, R., 2020. Effects of disturbance patterns and deadwood on the microclimate in European beech forests. Agric. For. Meteorol. 291, 108066. https://doi.org/10.1016/j.agrformet.2020.108066.

Tymen, B., Vincent, G., Courtois, E.A., Heurtebize, J., Dauzat, J., Maréchaux, I., Chave, J., 2017. Quantifying micro-environmental variation in tropical rainforest understory at landscape scale by combining airborne LiDAR scanning and a sensor network. Ann. For. Sci. 74 (2), 32. https://doi.org/10.1007/s13595-017-0628-z.

Van der Zande, D., Stuckens, J., Verstraeten, W.W., Mereu, S., Muys, B., Coppin, P., 2011. 3D modeling of light interception in heterogeneous forest canopies using ground-based LiDAR data. Int. J. Appl. Earth Obs. Geoinf. 13 (5), 792–800. https://doi.org/10.1016/j.jag.2011.05.005.

Vincent, G., Antin, C., Laurans, M., Heurtebize, J., Durrieu, S., Lavalley, C., Dauzat, J., 2017. Mapping plant area index of tropical evergreen forest by airborne laser scanning. A cross-validation study using LAI2200 optical sensor. Remote Sens. Environ. 198, 254–266. https://doi.org/10.1016/j.rse.2017.05.034.

Vincent, G., Pimont, F., Verley, P., 2021. Various PAD/LAD estimators implemented in AMAPVox 1.8. DataSuds V1. https://doi.org/10.23708/1AJNMP.

Vincent, G., Verley, P., Brede, B., Delaitre, G., Maurent, E., Ball, J., Clocher, I., Barbier, N., 2023. Multi-sensor airborne lidar requires intercalibration for consistent estimation of light attenuation and plant area density. Remote Sens. Environ. 286 (113442). https://doi.org/10.1016/j.rse.2022.113442.

Wang, Q.W., Pieristè, M., Liu, C., Kenta, T., Robson, T.M., Kurokawa, H., 2021. The contribution of photodegradation to litter decomposition in a temperate forest gap and understorey. New Phytol. 229 (5), 2625–2636. https://doi.org/10.1111/nph.17022.

Witzmann, S., Gollob, C., Kraßnitzer, R., Ritter, T., Tockner, A., Schume, H., Nothdurft, A., 2024. Modeling of solar radiation and sub-canopy light regime on forest inventory plots of mixed conifer and deciduous temperate forests using point clouds from personal laser scanning. For. Ecol. Manag. 569, 122166. https://doi.org/10.1016/j.foreco.2024.122166.

Xue, X., Jin, S., An, F., Zhang, H., Fan, J., Eichhorn, M.P., Jin, C., Chen, B., Jiang, L., Yun, T., 2022. Shortwave radiation calculation for forest plots using airborne LiDAR data and computer graphics. Plant Phenom. 2022, 1–21. https://doi.org/10.34133/2022/9856739.

Yang, X., Li, R., Jablonski, A., Stovall, A., Kim, J., Yi, K., Ma, Y., Beverly, D., Phillips, R., Novick, K., Xu, X., Lerdau, M., 2023. Leaf angle as a leaf and canopy trait: rejuvenating its role in ecology with new technology. Ecol. Lett. 26 (6), 1005–1020. https://doi.org/10.1111/ele.14215.

Yin, T., Qi, J., Cook, B.D., Morton, D.C., Wei, S., Gastellu-Etchegorry, J.P., 2020. Modeling small-footprint airborne lidar-derived estimates of gap probability and leaf area index. Remote Sens. 12 (1), 4. https://doi.org/10.3390/RS12010004.

Yoda, K., 1974. Three-dimensional distribution of light intensity in a tropical rain forest of West Malaysia. Jpn. J. Ecol. 24 (4), 247–254. https://doi.org/10.18960/seitai.24.4_247.

Zellweger, F., Baltensweiler, A., Schleppi, P., Huber, M., Küchler, M., Ginzler, C., Jonas, T., 2019a. Estimating below-canopy light regimes using airborne laser scanning: an application to plant community analysis. Ecol. Evol. 9 (16), 9149–9159. https://doi.org/10.1002/ece3.5462.

Zellweger, F., De Frenne, P., Lenoir, J., Rocchini, D., Coomes, D., 2019b. Advances in microclimate ecology arising from Remote sensing. Trends Ecol. Evol. 34 (4), 327–341. https://doi.org/10.1016/j.tree.2018.12.012.

Zellweger, F., De Frenne, P., Lenoir, J., Vangansbeke, P., Verheyen, K., Bernhardt-Römermann, M., Baeten, L., Hédl, R., Berki, I., Brunet, J., Van Calster, H., Chudomelová, M., Decocq, G., Dirnböck, T., Durak, T., Heinken, T., Jaroszewicz, B., Kopecký, M., Máliš, F., Coomes, D., 2020. Forest microclimate dynamics drive plant responses to warming. Science 368 (6492), 772–775. https://doi.org/10.1126/science.aba6880 (1979).